38th AIAA/ASME/SAE/ASEE Joint Propulsion Conference & Exhibit
7-10 July 2002, Indianapolis, Indiana

AIAA 2002-4149

VORTEX COMBUSTION CHAMBER DEVELOPMENT FOR FUTURE LIQUID ROCKET ENGINE APPLICATIONS

Martin J. Chiaverini,* Matthew J. Malecki,† J. Arthur Sauer,‡ and William H. Knuth§
Orbital Technologies Corporation (ORBITEC™)
Madison, WI 53717

ABSTRACT

A hot-fire test program using gaseous oxygen and hydrogen was conducted to characterize a laboratory-scale, cold-wall vortex combustion thrust chamber. Swirl oxidizer injection just upstream of the converging section of the nozzle generates a pair of coaxial, bi-directional vortices in the combustion chamber. Using proper head-end fuel injection methods and chamber geometry, propellant mixing and combustion may be confined to the inner vortex, while the outer vortex protects the chamber wall from excessive heat loads. Such thrust chambers can potentially reduce engine cooling requirements and possibly extend engine lifetimes. The results of the investigation indicated that, of the fuel injection techniques evaluated, the radial injector produced the best combination of performance and wall cooling behavior. Specific impulse efficiency of about 96% was achieved at a relatively low chamber pressure of about 150 psia, with higher performance expected from thrust chamber optimization efforts. The corresponding wall temperature increase was about 80 °C after 5 s of steady-state combustion. Initial higher pressure testing at about 400 psia also indicated cool chamber wall temperatures after 10 s of steady-state combustion.

NOMENCLATURE

Symbols

A	area
a_t	total speed of sound
C*	characteristic exit velocity
CR	contraction ratio
D	diameter
ID	inner diameter
I_s	specific impulse
L	length
L^*	characteristic chamber length
$\dot{m}$	mass flow rate
OD	outer diameter
O/F	mass mixture ratio
P	pressure
r	radius
r^*	nozzle throat radius
T	temperature

Greek Symbols

α	swirl parameter, Eq. 2
α^*	swirl parameter at nozzle throat
β	GOX split ratio, Eq. 3
γ	specific heat ratio
τ	thrust

Subscripts

a	axial
atm	atmospheric
c	chamber
e	exit
eff	efficiency
exp	experimental
o	oxidizer
sw	swirl
th	throat
tot	total
vac	vacuum
w	wall

INTRODUCTION

Many liquid-propellant rocket engine developmental issues arise from the large heat loads imposed on the thrust chamber surfaces by the combustion products of the fuel-oxidizer reaction. High heat loads may induce a variety of failure modes, severe thermal distress and fatigue, and injector face and exit nozzle deterioration. Techniques to alleviate these problems include regenerative, film, dump, transpirational, ablative, and radiation cooling as well as various combinations of these systems.[1] Each of these methods has been employed successfully for particular types of thrust chambers, yet are not necessarily appropriate for others. Regenerative cooling, for example, provides high performance, but may not be suitable where heat fluxes are high but large feed-system pressure drops cannot be tolerated.[2] Given that cooling requirements are intimately related to the selection of chamber pressure, and therefore the overall propulsion system performance? it seems beneficial to seek additional cooling techniques that may provide advantages for various types of liquid propulsion systems.

---

* Lead Propulsion Engineer, Space Center, 1212 Fourier Drive. Member AIAA.
† Propulsion Scientist, Space Center, 1212 Fourier Drive. Member AIAA.
‡ Aerospace Engineer, Space Center, 1212 Fourier Drive. Member AIAA.
§ Chief Engineer, Space Center, 1212 Fourier Drive. Associate Fellow AIAA.

The Vortex Combustion Cold-Wall (VCCW) chamber is an alternative approach that can potentially offer cooling benefits and additional design flexibility for liquid propellant thrust chambers. The key aspect of the design is a coaxial, co-spinning, but bi-directional vortex flow field that has been found to confine propellant mixing and burning to the core region of the chamber, thus alleviating wall heating via convection, chemical recombination, and thermal radiation. Figure 1 illustrates the overall concept.

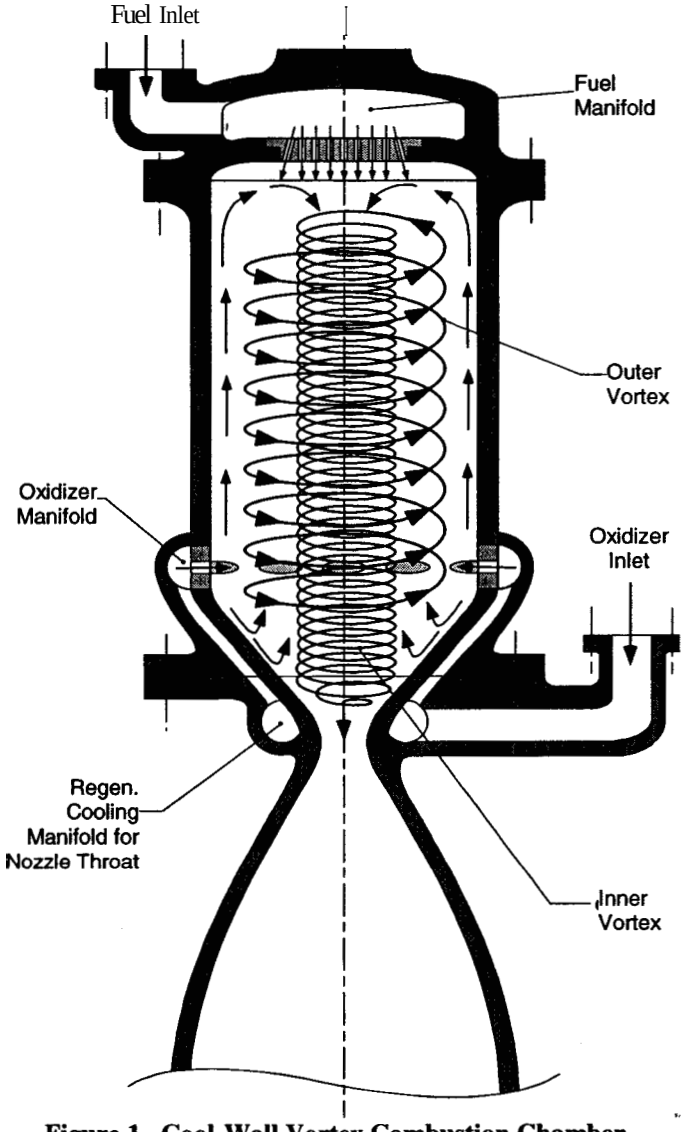

Figure 1. Cool-Wall Vortex Combustion Chamber Conceptual Design

An oxidizer swirl injection ring is located between the chamber spool section and the nozzle, while fuel injection occurs at the head-end. (Figure 1 shows a generic fuel injector for illustrative purposes.) Oxidizer injected through the swirl ring enters the chamber in a tangential manner, forming a vortex that spirals upwards along the chamber wall. The injected oxidizer is prevented from immediately flowing inward and out the nozzle by properly shaping the converging portion of the nozzle assembly and by the strong centrifugal forces associated with the tangential injection. At the faceplate, the outer vortex flows inward and forms a downward-spiraling inner vortex that exits the nozzle. Fuel is injected into the inner vortex where it is quickly vaporized and entrained by the swirling flow to ignite and burn with the oxidizer. Combustion is then confined to the inner vortex and the flow field thus prevents the hot combustion products from contacting the chamber wall. In addition, the outer vortex can cool the wall to alleviate the effects of thermal radiation. It should be noted that other cooling techniques, especially regenerative throat cooling and transpirational faceplate cooling, could be used in conjunction with the VCCW chamber. However, using vortex injection techniques could reduce the required coolant flow and decrease the overall turbopump pressure requirements.

The existence and basic features of the coaxial vortex flow field have been observed experimentally and predicted numerically. Figure 2 shows a video image of the lab-scale VCCW engine that was used to conduct the hot-fire experiments. Described more fully in the following sections, this engine sometimes employed a transparent acrylic test section for hot-firing flow visualization that was possible under particular test conditions due to the cold-wall operating characteristics. The photograph shows a side view image of a cylindrical combustion chamber burning **GOX** and GH_2 at a mixture ratio of 6 and a chamber pressure of about 135 psia. For scale, the outer diameter of the acrylic section is **3.5** inches. Notice that the combustion zone is confined to the inner region of the chamber by the coaxial flow field and that an annulus of non-combusting gas **(GOX)** separates the chamber wall surface from the combustion zone.

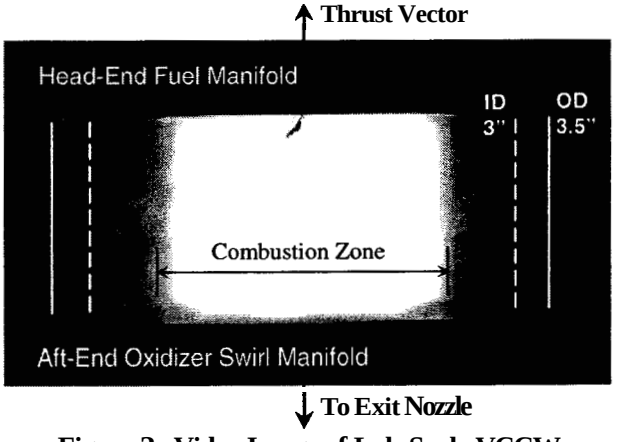

Figure 2. Video Image of Lab-Scale VCCW Chamber Showing Combustion Zone Confined to Inner Vortex

The VCCW concept grew out of ORBITEC's prior work with vortex-injection hybrid rocket engines.[3-5] Figure 3 shows a numerically-simulated velocity field for a 500-lb_f thrust vortex hybrid chamber. The CFD analysis was performed using the Finite Difference Navier Stokes (FDNS) code and is discussed fully in Ref. 3. The fuel port shown in Fig. 3 has a length and inner diameter of 9 in. (23 cm) and 5.25 in. (13.4 cm), respectively. The GOX flow rate is 1.35 lb_m/s (0.615 kg/s). The tangential oxygen injector is located just above the entrance to the convergent section of the nozzle in Figure 3. Though the wall is ablative solid fuel (HTPB) for the hybrid configuration, Figure 3 serves to illustrate the coaxial, bi-directional vortex flow field features discussed above for the VCCW.

The work described here was conducted under a NASA Phase I Small Business Innovation Research (SBIR) project to determine the technical feasibility of developing practical liquid propellant rocket engines based on the VCCW chamber. A Phase II SBIR project was recently awarded to continue the development of VCCW chamber technology. This article describes the primary findings of the Phase I effort and the preliminary results of the Phase II investigation.

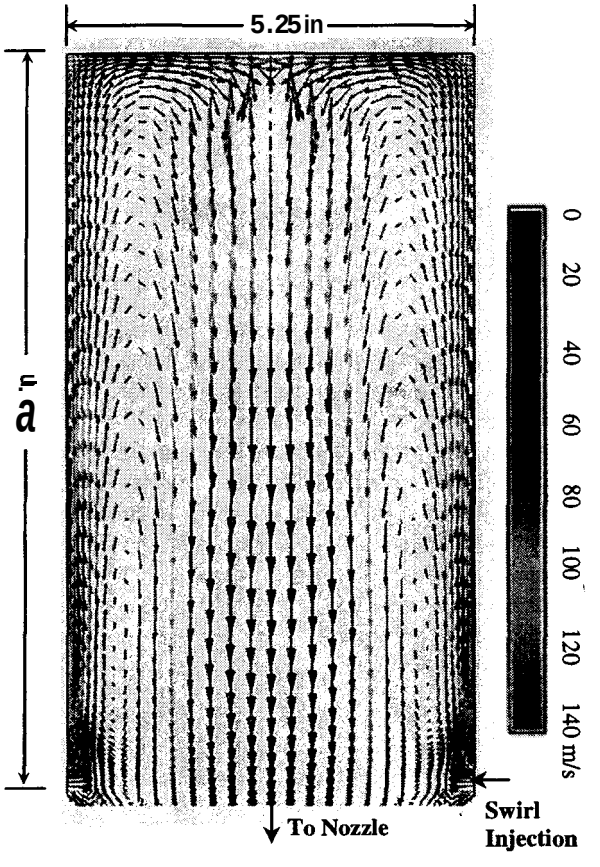

Figure 3. Velocity Field Predicted by FDNS Code for a 500-lb_f Vortex Hybrid Combustion Chamber

METHOD OF APPROACH

Thrust Chamber Hardware

Two lab-scale VCCW thrust chamber were designed with a modular style to provide flexibility in geometric variations and to accommodate various fuel injection methods. Most testing reported here was conducted at a 25 to 35 Ibf thrust range at chamber pressures of about 150 psia. However, some later tests were conducted at up to 400 psia. The nominal O/F mixture ratio was 6.

Figure 4 shows a assembly schematic of one of the thrust chambers in typical configuration with a radial fuel injector just below the chamber faceplate. This chamber accommodated components between 1 and 2 inches in inner diameter. A second, similar thrust chamber was used to test larger configurations with inner diameters from 2 to 3 inches. The GOX swirl injector was located upstream of the converging portion of the exit nozzle. Some testing also employed an auxiliary GOX injector located at the center of the faceplate. The propellant injectors were designed for pressure drops of about 10 to 15% chamber pressure.

In addition to the radial hydrogen injector shown in Figure 4, the fuel injector characterization test series considered: single axial jet injector located at engine centerline, dual axial jets located off-center (r=0.75 in), co-swirl injector (swirl direction same as GOX swirl direction), and counter-swirl injector (swirl opposite GOX swirl direction). The co-swirl, counter-swirl, and radial inflow injectors were all fabricated with four equally spaced injector ports. In addition to these methods, the co-swirl, counter-swirl, and radial injectors were also tested using auxiliary GOX injection through the single axial jet port in an attempt to enhance combustion in the central vortex.

The chamber length ranged from 1 to 3 inches. Chamber inner diameter of 1, 2, 2.5, and 3 inches were tested. The baseline nozzle throat diameter was chosen to be 0.5 in to obtain an approximate chamber pressure of about 150 psia. This chamber pressure was chosen so as not to induce severe stresses in the acrylic chambers that were used to conduct the experiments where optical visualization of the combustion field is of interest. Hot-fire testing up to about 400 psi was conducted using metallic chamber sections in order to obtain wall temperature data at somewhat higher chamber pressures. The baseline nozzle was a simple sonic throat design with no expansion section. This design facilitated the calculation of specific impulse efficiency from the thrust measurements by eliminating the effects of divergent nozzle losses. Several expansion sections were also fabricated for testing the chamber with converging-diverging nozzles. The diverging sections provided area ratio of 2, 3, and 4.

Engine instrumentation included: load cell for thrust measurements, a radial pressure transducer array at the chamber head-end, chamber wall pressure measurements, thermocouple array at the engine head end, and chamber wall and nozzle throat temperature measurements. Use of the transparent acrylic chambers also allowed for visual observation and recording of the combustion zone characteristics and diameter using standard video equipment and a digital video camera.

An augmented spark igniter was employed to ignite the main propellant flow in the combustion chamber. The igniter gases entered the chamber through a port in the faceplate.

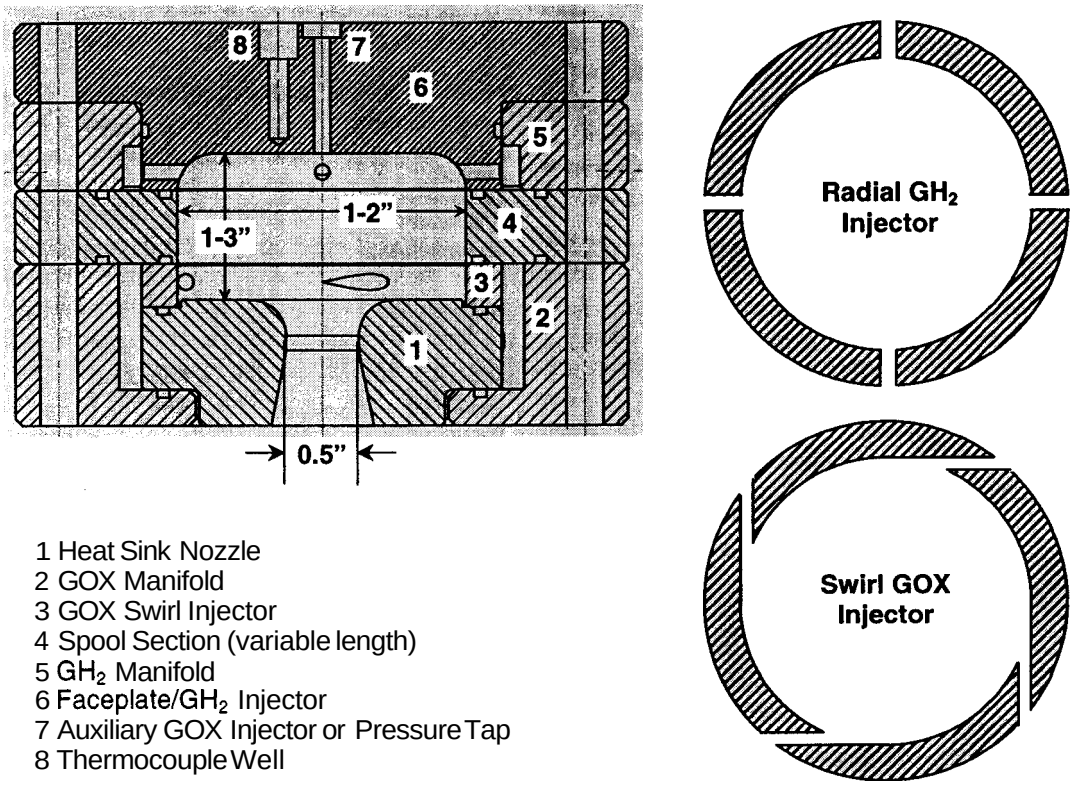

Figure 4. Lab-Scale VCCW Thrust Chamber Assembly

Thrust Chamber Performance Analysis

The specific impulse efficiency was used as the primary measure of thrust chamber performance and was calculated by comparing the experimentally determined specific impulse at ambient conditions to the theoretical equilibrium ambient specific impulse based on calculations using the CEA code developed at NASA/GRC.[6] The CEA code provides both vacuum and optimum specific impulse values for a given set of propellant mixture ratio, chamber pressure, and area expansion ratio values. Since the lab-scale test engine did not necessarily provide optimum expansion ($P_e=P_{atm}$) the theoretical specific impulse values were found by subtracting the effect of atmospheric pressure acting on the exit area from the theoretical vacuum specific impulse. The specific impulse efficiencies (in %) were calculated using:

$$I_{sp,eff} = 100 \times \frac{\tau_{exp}/\dot{m}_{tot}g}{\left[I_{sp,vac} - \frac{P_{atm}A_e}{\dot{m}_{tot}g}\right]} \qquad (1)$$

where the numerator represents the experimental I_{sp} based on thrust measurements and the denominator is the corresponding theoretical I_{sp} at ambient conditions. An averaging procedure was used over the steady-state portion of the thrust and propellant line pressure profiles to determine thrust and flow rates used in the calculations. The overall engine system demonstrated very little transient behavior after the ignition and propellant ramp interval. Typical propellant ramp intervals were about 1 s, followed by about 5 to 6 s of steady-state operation. A few longer duration tests of up to 10 s steady-state operation were conducted.

It has been well established in the literature that swirling flow can influence nozzle flow and subsequent performance for a variety of applications.[7-14] Mager[8] developed closed-form solutions to approximate isentropic swirling flow through nozzles for gases with specific heat ratios of 1.4. An analysis based on this procedure, but modified for different specific heat ratios, was conducted to determine the effects of swirling flow on vortex thrust chamber performance.

Based on chemical equilibrium calculations a specific heat ratio of **1.125** was adopted for the analysis for the combustion of GOX and GH_2.

Mager's analysis produced closed-form, algebraic equations with which to calculate the reductions in thrust and specific impulse associated with swirl flow, assuming that the vortex flowing through the nozzle was a potential (irrotational) vortex. Other researchers, such as Lewellen et al.,[9] performed subsequent work for mixed vortices having arbitrary amounts of rotation. Since the extent of rotation was not known a priori for the vortex combustor of interest here, Mager's analysis was adopted to provide a preliminary estimate of the effect of swirl flow on nozzle performance. His analysis is presented in detail in Ref. 8 and will not be repeated here. However, it is useful to present the definition of the swirl parameter that appears in Mager's equations. The relative strength of the swirl flow can be characterized by a non-dimensional parameter, α, defined by

$$\alpha(x) = \left(\frac{K_1}{r\, a_t}\right)\sqrt{\frac{\gamma - 1}{2}} \qquad (2)$$

which in general is a function of axial distance, x, along the nozzle. For the current analysis, the value of α at the throat, α^*, is of primary interest as a convenient reference dimensionless swirl strength and also because most of the hot firings reported here were conducted using a truncated nozzle (no expansion section). In this case, r is equal to the throat radius, r^* (**0.25** in. for the current chamber). The parameter K_1 is a constant equivalent to the angular momentum of the swirl flow and can be calculated from the known chamber geometry, GOX swirl injection momentum, and GH_2 injection method. Note that, depending on the fuel injection technique, the hydrogen momentum can be effectively neutral (axial or radial injection), positive (co-swirl), or negative (counter-swirl).

The results of the analysis showed that for the relatively low throat swirl numbers (about 0.1) encountered during this investigation, swirl flow has very little effect on thrust chamber performance. For a typical throat swirl number of **0.1,** the specific impulse is theoretically reduced by about **1%** compared to the case of non-swirling flow. This value is smaller that the error on the experimental I_{sp} calculation, which was estimated to be about **+/- 2%.**

It is also worth noting from Mager's analysis that swirl flow has the greatest effect on the performance of a truncated nozzle (no expansion). Reference 8 shows that the effect of swirl becomes smaller, and eventually negligible, as the nozzle area expansion ratio increases. This behavior results from both conservation of angular momentum, which requires that tangential velocity decrease as nozzle radius increases, and supersonic flow behavior, in which velocity increases as flow area increases. As nozzle exit area increases, the axial velocity increases and the tangential velocity decreases, and the relative magnitude of the tangential-to-axial velocity decreases rapidly. For a nozzle area ratio of about **10,** Mager's analysis indicates that the effect of swirl on specific impulse becomes entirely negligible for values of α^* less than about 0.3. In comparison, a 10,000 lb_f thrust, 1000 psi, vortex combustion chamber employing tangential LOX injection at a velocity of about **100 ft/s** is expected to have an approximate α^* of about **0.01,** assuming a typical L* of 30 in. and a contraction ratio of **4.8.** The I_{sp} loss resulting from swirl flow is theoretically about 0.04% for this case. Though these results are approximate due to the somewhat uncertain degree of rotation in the exit nozzle flow, they suggest that swirl flow should not cause any significant performance degradation for practical rocket engine propulsion systems employing vortex combustion chambers.

The efficiency of the characteristic exit velocity, C^*_{eff}, was not employed as a primary performance metric because the vortex flow field present in the combustion chamber generates radial pressure gradients that complicate the determination of an average chamber pressure for calculating experimental C^* values. In addition, swirl flow can reduce the effective nozzle throat area', further complicating the analysis of C^* efficiency. An analysis similar to that discussed above for the I_{sp} efficiency was conducted for a limited number of tests that had well-characterized radial pressure gradients for calculating the average chamber pressure. (The head-end pressure transducer array was not available for all chamber configurations due to the particular fuel injector and faceplate geometry.) The results of the analysis indicated C^* efficiencies of about **94** to 99% for the tests that also demonstrated high $I_{sp,eff}$.

RESULTS AND DISCUSSION

Several series of hot firings were conducted to characterize the performance and heating behavior of the lab-scale VCCW thrust chambers. Gaseous oxygen (GOX) and hydrogen (GH_2) were used in all cases. Test Series A consisted of ignition and system check out tests which did not yield reportable data. Series B represented the bulk of the test effort and focused on characterizing the performance of various fuel injection techniques. The effect of injecting a portion of the GOX through the axial jet to enhance combustion in the inner vortex was investigated during Series C. Test Series D focused on the affects of chamber geometry on thrust chamber performance and wall cooling. A limited number of higher-pressure, longer-duration tests were also conducted.

Fuel Iniector Characterization Testing (Test Series B)

The fuel injection techniques were compared and evaluated using metrics of specific impulse efficiency and wall and faceplate temperature. Nozzle throat temperature was also measured but not used as a primary means of evaluation since no attempt was made to cool the nozzle throat during this initial investigation.

All fuel injector characterization tests were conducted with a 3-inch overall chamber length and 3-inch inner diameter. The radial, co-swirl, and counter-swirl injectors had variable inner diameters to allow the radial location of the hydrogen injection ports to be changed with respect to the radial location of the GOX swirl injection ports (which were always flush with chamber inner wall). These three families of fuel injectors were also tested with the addition of 10%of the total gaseous oxygen flow injected through the central head-end axial port to assist in burning the gaseous hydrogen in the center vortex region. The *total* oxygen flow, and therefore the overall mixture ratio, was maintained at a nearly constant value throughout the test program. However, no attempt was made to maintain a constant pressure drop across the GOX swirl injector for the different swirl GOX flow rates.

Figure 5 compares the specific impulse efficiencies of the various fuel injection techniques arranged in terms of injector class: axial injectors, co-swirl injectors, counter-swirl injectors, and radial injectors. The data trends lead to several significant findings. First, the axial jet injector had by far the worst performance in terms of specific impulse efficiency of all injectors tested. It is theorized that aligning the injector in the center of the inner vortex allows a large portion of the fuel to pass through the low-pressure vortex core and out the nozzle without mixing and burning with the GOX. Swirl injection of oxygen creates centrifugal forces in the flow field that tend to force the relatively high molecular weight oxygen toward the wall and the light hydrogen gas toward the center of the combustion chamber. When injected through the center of the faceplate, the hydrogen gas may flow along the vortex core toward the nozzle without mixing adequately with the oxygen. Employing dual axial jets of hydrogen through injectors located 180 deg. apart at radii of 0.75-inch (halfway to the chamber wall) improved performance significantly. This method probably improved mixing and also provides a longer flow path for combustion since the fuel is introduced into the oxygen stream at a greater radius and at a location where the oxygen swirl velocity and shear strength are higher.

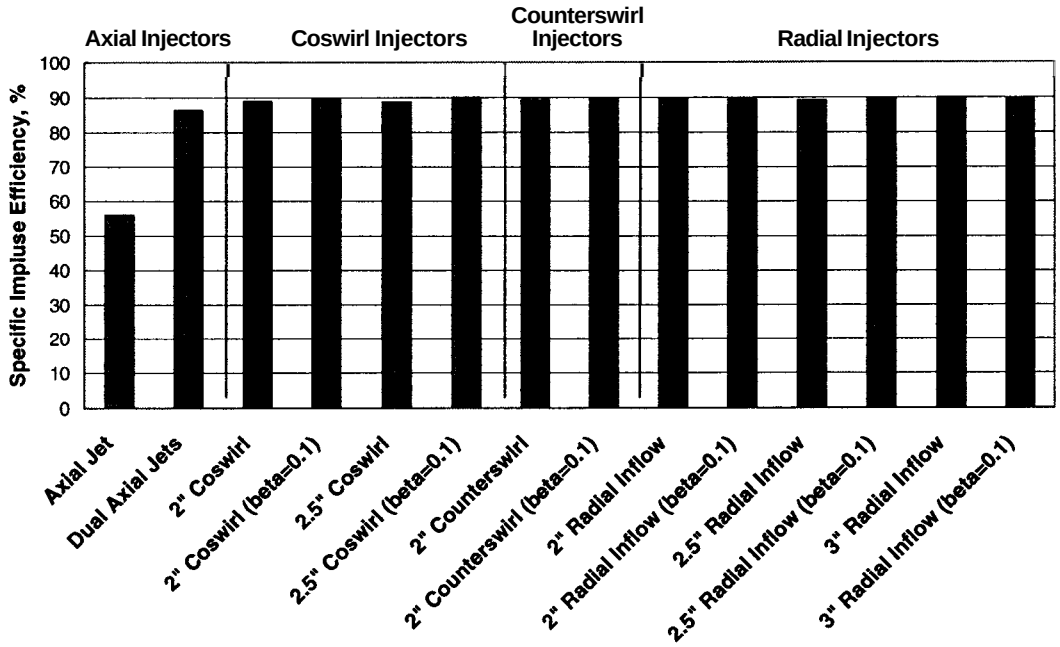

Figure 5. Specific Impulse Performance of Various Fuel Injectors

The fuel co-swirl, counter-swirl, and radial injection methods all had similar specific impulse efficiencies of about 90%. (Higher efficiencies were obtained for different chamber geometries and will be discussed later.) The radial and co-swirl injectors may improve performance by increasing the reaction zone diameter, thus providing a longer effective path length for mixing and combustion to occur. Counter-swirl fuel injection probably enhances propellant mixing by impinging the propellant streams at the wall. For these three injector

types, the injection of 10% of the total oxygen flow through the central jet injector, indicated by the label "β=0.1" improved performance only slightly. Additional testing using larger GOX split ratios between the swirl and auxiliary injector will be discussed later.

Though the co-swirl, counter-swirl, and radial injectors all produced similar specific impulse results, the corresponding chamber heating behavior varied significantly, as is evident from the wall temperature profiles. Figures 6 and 7 show the chamber wall temperature profiles for the various fuel injection techniques for wall temperatures greater than 100 °C, and less than 100 °C, respectively. The wall temperatures represented in these figures were measured at midway along the spool section. However, very little axial variation in wall temperature, on the order of 10 °C along the length of the chamber, was observed.

Figure 6 indicates that the counter-swirl fuel injector resulted in the highest wall temperature, 562 °C, of all the fuel injectors tested. In addition, the temperature profile is relatively steep, indicating that the wall surface was not approaching a steady-state value and would continue to increase for longer test times. The counter-swirl injector disrupts the vortex flow pattern since fuel is injected tangentially opposite to the GOX swirl. Therefore, the swirling GOX is not effective in cooling the wall and does not protect the chamber from relatively large surface heat fluxes.

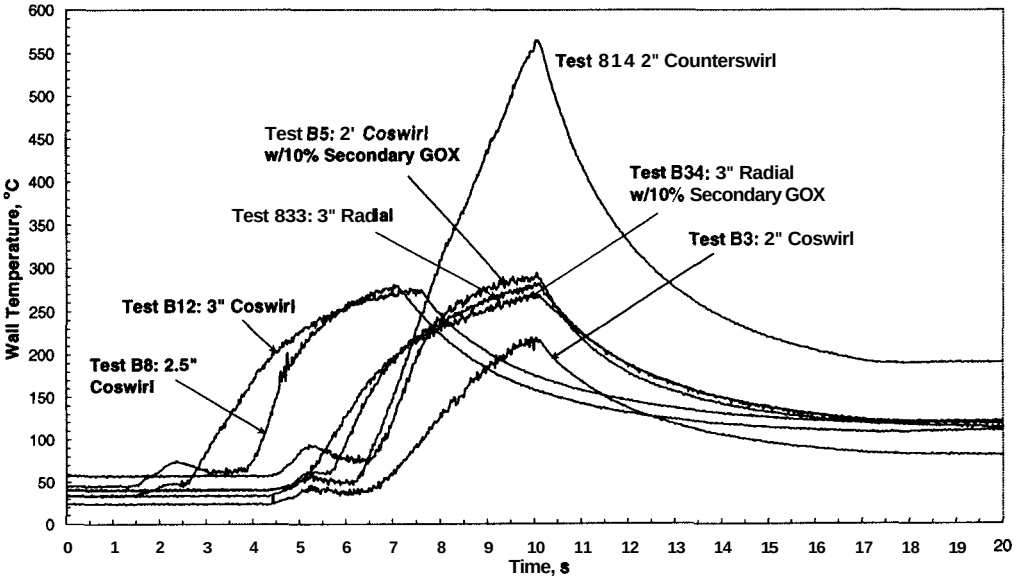

Figure 6. Wall Temperature Profiles for Various Fuel Injectors ($T_{w,max}$ > 100 °C)

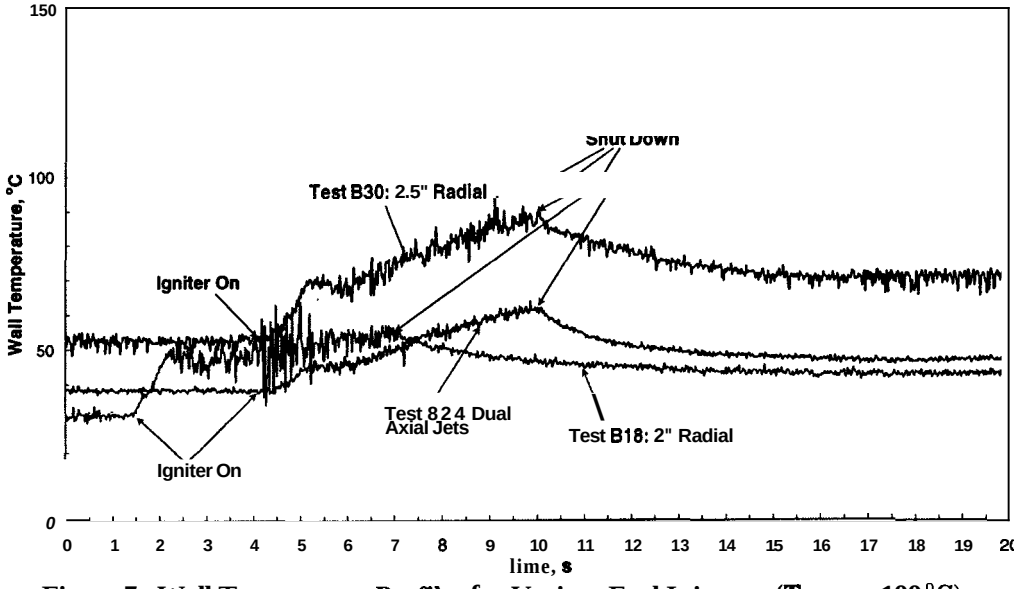

Figure 7. Wall Temperature Profiles for Various Fuel Injectors ($T_{w,max}$ < 100 °C)

The co-swirl fuel injectors had lower wall temperature profiles than the counter-swirl, as indicated in Figure 6. Unlike the counter-swirl injectors, the co-swirl injectors do not act to disrupt the outer vortex of oxygen that protects the chamber wall. Of the three co-swirl fuel injectors tested, the 2-inch diameter injector resulted in the lowest wall temperature. Using a smaller fuel injector diameter probably confines the reaction zone to a smaller radial region, thus separating the flame from the wall. Use of auxiliary oxygen through the axial injector results in a higher wall temperature, probably due to reduced cooling capacity (similar results were obtained for the counter-swirl injector, but are not shown in Figure 7). It is also interesting to note that there is little difference between the 2.5-inch co-swirl fuel injector and the 3-inch co-swirl fuel injector that is flush with the chamber wall.

The 3-inch radial injector, with hydrogen injected at the wall, displayed wall temperatures similar to those of the co-swirl injectors. However, auxiliary oxygen injection had no significant effect on the resulting wall temperature, in contrast to the results obtained for the co-swirl and counter-swirl injectors.

As shown in Figure 7, the 2-inch and 2.5-inch radial injectors had much lower wall temperatures, below 100 °C. The 3-inch injector had higher wall temperatures than the other radial injectors because the fuel enters the chamber flush with the chamber wall. This arrangement may allow the reaction zone to reside closer to the wall than for the other cases, thus increasing the wall temperature. It is also important to note that hot-fire testing with transparent acrylic for flame zone visualization could not be achieved using the 3-inch radial inflow injector (flush with the chamber inner diameter) without igniting the chamber wall. Similar results were achieved with the co-swirl and counter-swirl injectors. In contrast, the 2-inch and 2.5-inch radial inflow injectors were successfully employed for hot-fire flow visualization testing with a 3-inch chamber.

Figure 8 shows video images from these tests. Rough approximations of the extent of the visible flame zone were made for each case using the outer diameter of the acrylic chamber, 3.5 in, as a reference scale. The inner diameter of the chamber, as well as the approximate location of the radial GH_2 injection ports, are indicated on the photographs. Though it is difficult to make very precise measurements using this method, a relative comparison of the approximate diameter of the visible combustion zone is interesting. In Fig. 8a, the visible combustion zone diameter was estimated at approximately 1.6 in. The inner diameter of the fuel injector is slightly larger at 2 in. Similarly, the test shown in Fig. 8b indicates a visible combustion zone diameter of roughly 2.1 in – slightly smaller than the fuel injector inner diameter of 2.5. These results indicate qualitatively that, for the radial fuel injection method, the flame zone diameter can potentially be controlled by varying the radial location of the injector with respect to the chamber inner diameter. This behavior may have implications for VCCW chambers since it may be possible to optimize combustion efficiency and cool wall operation by controlling the combustion zone diameter.

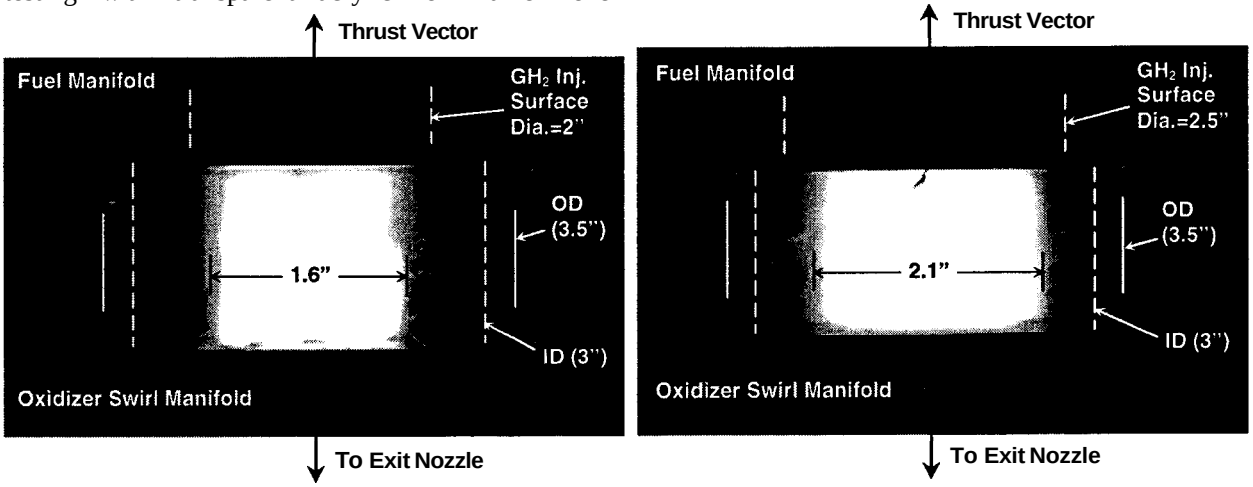

a) 2-inch Radial Inflow b) 2.5-inch Radial Inflow

Figure 8. Hot-Firing Flow Visualization Tests in Acrylic Chambers Showing Visible Combustion Zone

GOX Injection Split Ratio Testing (Test Series C)

The radial fuel injector was chosen for additional testing based on its desirable combination of relatively high performance and cool wall operation. Testing focused on determining the effects of injecting varying portions of the GOX through the auxiliary injector to mix with unburned fuel in the core region. Experiments were performed using a 2-inch diameter, 2.2-inch long chamber rather than the 3"x3" chamber used for the fuel

injection characterization testing because initial chamber geometry tests, discussed later, had already indicated that performance increased as chamber size was reduced. The corresponding L^* and chamber area contraction ratio were 35.2 in and 16, respectively. The main GOX flow was injected through a 2-inch ID tail-end swirl injector while a 2-inch ID head-end radial inflow fuel injector was used to inject the GH_2. The central faceplate axial injector was used for auxiliary oxygen injection. The oxidizer split ratio was varied between 0 and 0.38 (target values of 0 to 0.40). The split ratio, β, is defined as the mass flow rate of oxygen injected through the central faceplate port with respect to the total oxygen mass flow rate into the chamber:

$$\beta = \frac{\dot{m}_{o,a}}{\dot{m}_{o,a} + \dot{m}_{o,sw}} \qquad (3)$$

where $\dot{m}_{o,a}$ is the GOX mass flow through the face plate axial jet and $\dot{m}_{o,sw}$ is the GOX mass flow rate through the main swirl injector. No attempt was made to control either the swirl or axial injection velocities at a constant value. Therefore, changing the swirl oxygen flow rate necessarily resulted in different oxygen swirl and axial injection velocities. Future work will employ a family of GOX swirl and axial injectors such that the velocities remain fixed while the split ratio is varied. Such a procedure can isolate the effects of swirl momentum and split ratio on performance.

Figure 9 shows the specific impulse results of the GOX split ratio testing. The specific impulse efficiency peaks at 92.7% at a β of 0.19. At β values above this level, the performance decreases.

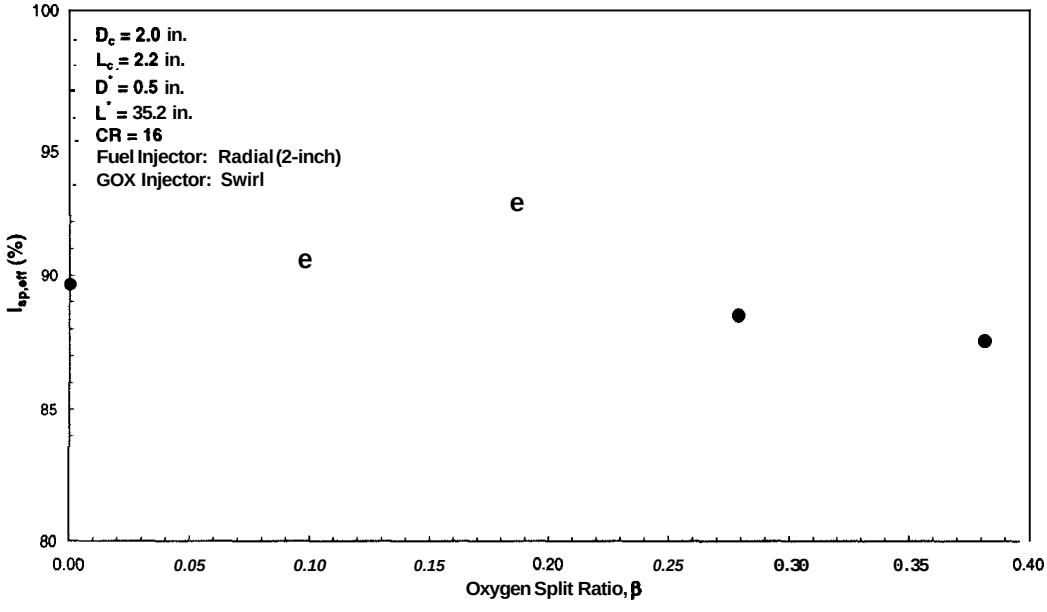

Figure 9. I_{sp} Efficiency vs. β for Nominal Radial Fuel Injector Configuration

A possible explanation for this behavior concerns the mixing and combustion processes in the coaxial flow field. As the amount of auxiliary GOX increases from 0 to about 20%, the oxygen injected into the core vortex may increase specific impulse efficiency by enhancing the combustion of hydrogen in the core vortex. However, at split ratios greater than 0.2, reduced mixing may accompany the decrease in GOX swirl momentum and lead to lower combustion efficiency. In addition, the increase of auxiliary GOX velocity at higher split ratios may have a detrimental effect on mixing and combustion in the vortex core by forcing the combustible mixture out the nozzle before reactions are completed.

It is also interesting to investigate the effects of GOX split ratio on chamber temperature behavior by examining the data shown below in Table 1.

Table 1. Test Series C Wall Temperature Results

Test	GOX β, %	Swirl GOX ΔP_{inj}, %Pc	AT_w °C	Average $\Delta T_w/\Delta t$ °C/s
C1	0	18.2	79.6	14.5
C2	9.8	14.8	78.0	14.2
C4	18.6	13.0	94.1	17.1
C5	27.9	10.9	93.5	17.0
C6	38.2	7.1	87.3	15.9

Notice that the change in wall temperature from ambient conditions remains relatively low over the range of β values despite the decrease in GOX swirl pressure drop, and therefore GOX injection velocity, as β increases. The average wall temperature increase over the steady-state test time also varies little for the different split ratios, have an approximate value of about 15 deg C/s.

These data imply that adequate wall cooling was achieved at GOX swirl injector pressure drops as low as 7% of chamber pressure. Additional testing must be conducted to determine if similar results can be achieved at higher chamber pressures.

Chamber Geometry Variation Testing (Series D)

The effects of chamber geometry on performance and heat transfer behavior were also investigated for the radial fuel injector configuration. Chamber geometry tests were performed by varying the chamber diameters (1, 2, 2.5, and 3 in.) and the chamber lengths (2-3 in.). Based on the results and interpretations of the split ratio testing, the secondary oxygen flow rate through the central faceplate axial injection port was set at 20% of the total oxygen flow rate. In some cases, tests were conducted using β=0 and β=0.2 for the same geometry to directly compare the results. A limited number of tests using a hemispherical faceplate in place of the nominal flat faceplate were also conducted. The hemispherical faceplate had a 1 inch radius and was tested in the 2-inch diameter chamber. The radial fuel injector was located just forward of the base of the hemisphere for this configuration.

Figures 10 through 12 summarize the results of this test series in terms of $I_{sp,eff}$ and wall and faceplate temperature histories. Figure 10 illustrates the variation of $I_{sp,eff}$ as a function of characteristic chamber length, L^* for two values of β, where L^* is defined in the conventional sense of chamber volume, V_c, divided by throat area, A_{th}. The contraction ratio of each group of data is also indicated ($CR=A_c/A_{th}$). As discussed in the previous section, a split ratio of about 20% gave higher performance than the baseline case of no secondary GOX. This effect is more pronounced at smaller values of L^* and contraction ratio and is probably due to improved propellant mixing in the core vortex.

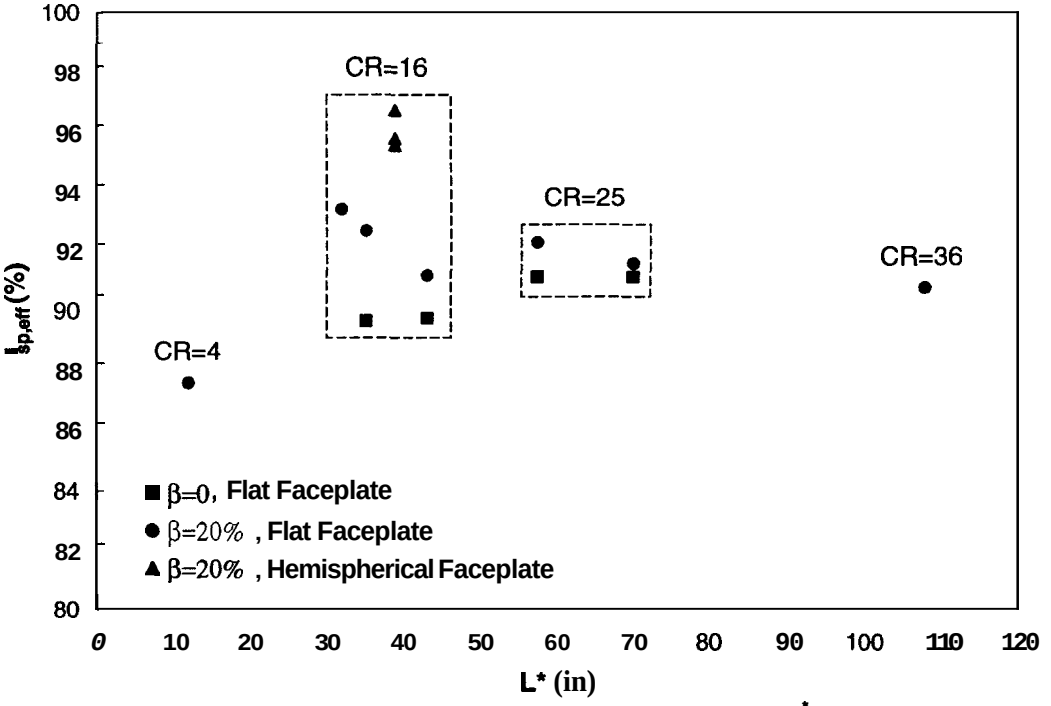

Figure 10. Variation of Specific Impulse Efficiency with L^* and CR

Another interesting result indicated in Figure 10 is that performance appears to improve slightly at lower L^* values down to an L^* of about 30 to 40. Values of $I_{sp,eff}$ of about 94% and 96% were measured for the flat and hemispherical faceplate, respectively. This effect may result from injecting the hydrogen and oxygen in closer proximity as the chamber size is decreased, thus improving mixing. A decrease in performance was measured for the minimum L^* of 12 in. tested in the 1-inch diameter chamber configuration. However, future experiments must be conducted to determine if this behavior is due to a low L^* value or a low contraction ratio. In addition, testing in the range of L^* between 15 and 30 in. must be conducted to determine where performance begins to decrease for a given pressure and contractionratio.

The higher performance of the hemispherical faceplate over the nominal flat faceplate (see Fig. 4) may be due to enhanced propellant mixing in the chamber volume upstream of the fuel injector. The flat faceplate provides very little chamber volume downstream of the fuel injector, whereas the hemispherical faceplate geometry may allow for a larger amount of propellant mixing prior to entering the core vortex.

Both the maximum chamber wall and faceplate temperatures tended to decrease as the chamber L^* was reduced, as shown in Figures 11 and 12. More effective wall cooling may result from smaller chamber surface area to be cooled, as well as a relatively higher angular velocity of fluid in the outer vortex as chamber diameter is decreased for a given GOX tangential injection velocity. Higher angular velocity implies a larger number of revolutions per unit length of chamber wall as the outer vortex spirals toward the faceplate. This phenomena may improve the wall cooling effect. In addition, a comparison of the trends shown in Figure 11 indicate that shorter chambers also have lower wall temperature (Test D5 vs. D6), possibly due to smaller exposed surface area to receive thermal radiation from the flame zone. Test C1, which had the smallest chamber volume, also displayed a temperature trace that appears to be nearing a steady-state temperature of about 110°C after a test time of about 5 seconds. The other traces display higher heating rates.

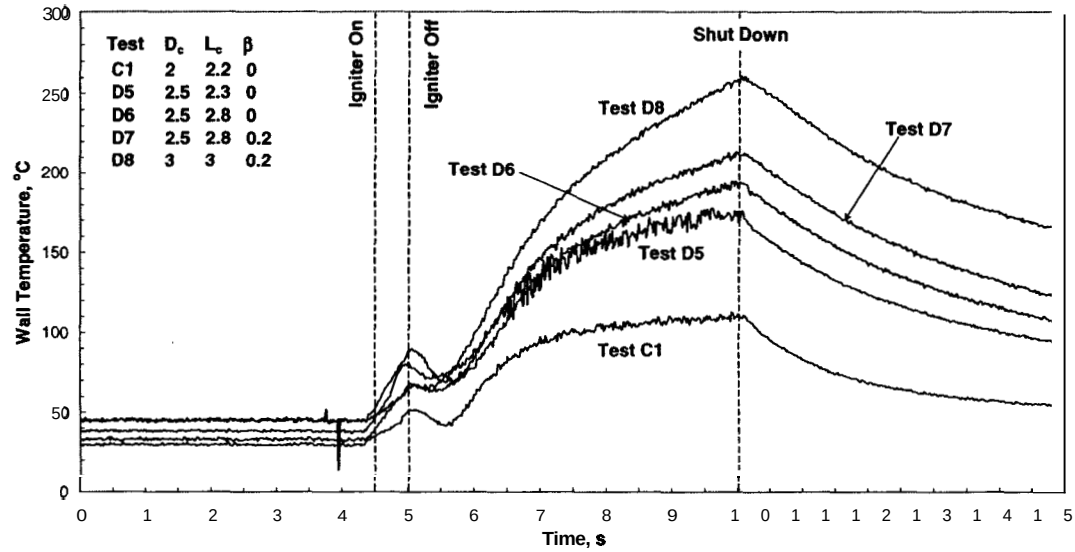

Figure 11. Wall Temperature Histories for Various Chamber Geometries and Split Ratios

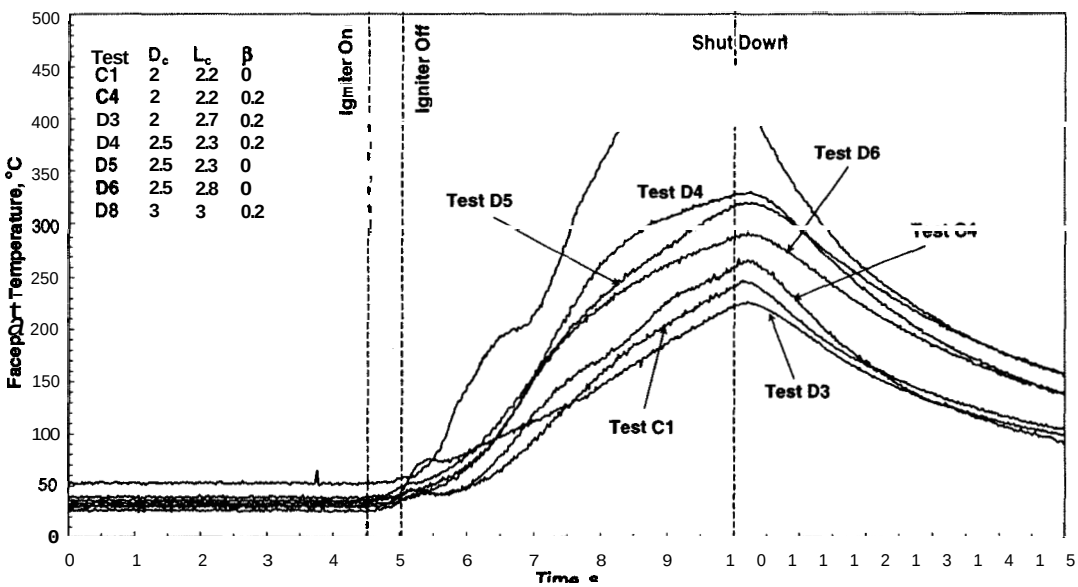

Figure 12. Face Plate Temperature Histories for Various Chamber Geometries and Split Ratios

The faceplate temperatures were measured at several radial locations, but were consistently highest at the innermost location of 0.77 in from the faceplate center. These measurements are shown in Figure 12. Faceplate cooling may improve for smaller diameters because of stronger vortex flow across the faceplate, which results from lower momentum dissipation as the outer vortex moves up the chamber wall and across the faceplate. In addition, smaller faceplate surface area may lead to lower temperatures. Note also from Fig. 12 that for

tests of the same geometry (e.g. Test C1 and C4, and D4 and D5) faceplate temperatures tended to be higher when auxiliary oxygen was employed. Enhanced combustion in the core vortex may contribute to this behavior.

Higher-Pressure Test Results

To provide preliminary data on vortex combustion performance and chamber heating at higher pressures, the lab-scale VCCW chamber was modified slightly to accommodate higher propellant flow rates. A series of tests were conducted using GOX and GH_2 at increasing higher chamber pressures. In addition, a longer duration test firing of 10 s steady state combustion was conducted (11.5 s total between ignition and shut down). Due to limitations of the propellant flow rate venturi sizes available for the testing, mixture ratios were limited to about 4.5. Future work is planned with additional flow control venturis for testing at both higher mixture ratios and higher thrust levels. The thrust chamber was tested using a combustion chamber of 2 in. ID and 2.2 in. length with a 0.5-inch nozzle throat. Cooling water was sprayed directly onto the rear face of the truncated exit nozzle near the throat to prevent thermal degradation at the higher pressures. No reportable specific impulse efficiencies were obtained due to a malfunction with the facility load cell system.

Typical results of the higher-pressure testing are shown in Figure 13. The tests indicated that cool chamber walls, on the order of 100 °C, could be maintained at higher pressures up to nearly 400 psia, the highest pressure tested. Notice that the wall temperature trace appears to approach a steady-state temperature of less than 100 °C after a test time of about 10 s. Faceplate temperature were similar to those measured in the lower-pressure tests and indicated higher heating rates than the wall temperatures. While it may be expected that chamber wall, faceplate, and nozzle throat would display slightly higher temperatures at a higher mixture ratio of about 6 due to the increased flame temperature, these results serve to indicate that cool-wall operation is possible at higher pressures. Future work will examine the effects of wall heating at higher chamber pressures and mixture ratios.

Note also from Figure 13 that the VCCW thrust chamber displays smooth combustion with pressure oscillations of about +/- 5 psi, or about 1.25% P_c. Similar results were also obtained for the hot-fire tests discussed previously. No significant pressure oscillations or combustion instability were observed during the hot-fire test program. The pressure traces shown in Fig. 13 also indicate the vortex flow characteristic of radial pressure gradients.

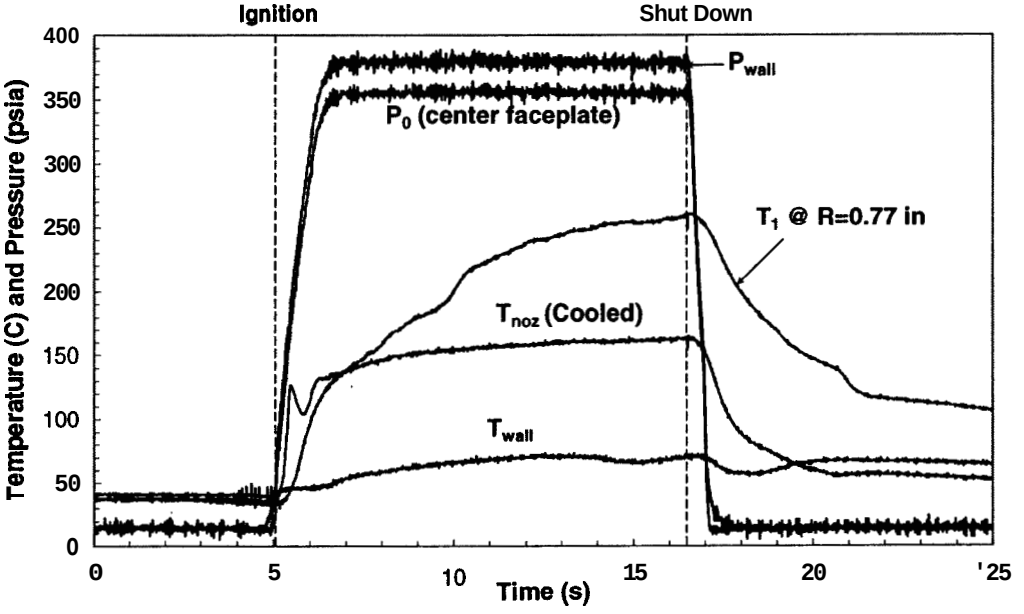

Figure 13. Typical Chamber Pressure and Temperature Traces for Higher-Pressure Test Series

SUMMARY AND CONCLUSIONS

The main purpose of this work was to determine the feasibility of employing a coaxial vortex flow field to develop cold-wall vortex combustion chambers for liquid propellant rocket engine applications. The coaxial vortex flow field is generated by injecting oxidizer through a swirl ring located at the base of the combustion chamber just upstream of the exit nozzle. A modular, lab-scale thrust chamber assembly was tested to determine the effects of fuel injection method and chamber geometry on I_{sp} performance and chamber wall temperature behavior. Major results of the investigation include:

- The radial GH_2 injector had the most desirable behavior in terms of wall cooling and specific impulse efficiency of the fuel injection methods examined during the investigation
- Use of an auxiliary jet of oxygen directed along the chamber centerline improved specific impulse performance by enhancing combustion in the core vortex
- Specific impulse efficiency of 96% was obtained at relatively low pressure of about 150 psia
- Cool-wall operation was demonstrated at chamber pressures of nearly 400 psi (the maximum tested)
- Not significant pressure oscillations or combustion instabilities were observed or measured.

Though these results are promising, additional work is required to mature VCCW technology for higher chamber pressures and larger thrust levels. In addition to size scale-up, potential issues include the effects of thermal'radiation on wall and faceplate heating rates at elevated pressures and determining the amount of residual torque on the vehicle. A Phase I1 SBIR project has recently been initiated to continue the development of vortex combustion chamber technology for NASA Marshall Space Flight Center. The program focuses on testing larger-scale thrust chambers at pressures of 1000 psi and thrusts of 500 to 1250 lb_f using GOX/GH_2 and LOX/GH_2. Additional efforts include numerical simulations of the vortex flow field using CFD analysis, development of analytic techniques to approximate the flow field characteristics, and the design of larger thrust chambers for future applications.

ACKNOWLEDGEMENT

This work was performed under a NASA Phase I SBIR project, contract no. NAS8-01073. The support and encouragement of Mr. Huu Trinh, NASA Marshall Space Flight Center's Technical Monitor, is gratefully acknowledged. The authors also gratefully acknowledge the support and encouragement of Dr. John Hutt and Mr. Steve Cook, NASA/MSFC.

REFERENCES

1. Sutton, G.P., ***Rocket Propulsion Elements,*** 6" ed., John Wiley & Sons, New York, 1992, pp. 109-116, 289-294.
2. Huzel, D.K., and Huang, D.H., *Modern **Engineering for Design of Liquid-Propellant Rocket Engines,*** AIAA Progress in Aeronautics and Astronautics, Vol. 147, 1992, pp. 84-104.
3. Knuth, W.K., Chiaverini, M.J., Sauer, J.A., and Gramer, D.J., "Solid-Fuel Regression Rate Behavior of Vortex Hybrid Rocket Engines," *AIAA **Journal of Propulsion and Power*** Vol. 18, No. 3, 2002, pp. 600-609..
4. Knuth, W.H., Chiaverini, M.J., Gramer, D.J., and Sauer, J.A., "Experimental Investigation of Vortex-Driven, High-Regression Rate –Hybrid Rocket Engines," AIAA Paper 98-3348, 34" Joint Propulsion Conference, Cleveland, OH, July 1998.
5. Knuth, W.H., Gramer, D.J., Chiaverini, M.J., Sauer, J.A., Whitesides, R. H., and Dill, R. A., "Preliminary CFD Analysis of the Vortex Hybrid Rocket Chamber and Nozzle Flow Field," AIAA Paper 98-3351, 34" Joint Propulsion Conference, Cleveland, OH, July 1998.
6. McBride, B. J., and Gordon, S., *Computer Program **for Calculation of Complex Chemical Equilibrium Compositions and Applications,*** NASA Reference Publication 1311, NASA John H. Glenn Research Center at Lewis Field, Cleveland, OH, June 1996.
7. Goldman, C. and Gany, A., "Thrust Modulation of Ram-Rockets by a Vortex Valve," AIAA Paper 96-2624, 32nd Joint Propulsion Conference, Lake Buena Vista, FL, July, 1996.
8. Mager, A., "Approximate Solution of Isentropic Swirling Flow Through a Nozzle," ***American Rocket Society Journal,*** Vol. 31, No. 8, 1961, pp. 1140-1148.
9. Lewellen, W.S., Bums, W.J., and Strickland, H.J., "Transonic Swirling Flow," ***AIAA Journal,*** Vol. ***7,*** No. 7, July 1969, pp. 1290-1297.
10. Bastress, E.K., "Interior Ballistics of Spinning Solid-Propellant Rockets," Journal ***of Spacecraft and Rockets,*** Vol. 2, NO. 3, May-June 1965, pp. 455-457.
11. Batson, J.L. and Sforzini, R.H., "Swirling Flow Through a Nozzle,'' ***Journal of Spacecraft and Rockets,*** Vol. ***7,*** No. 2, February 1970, pp. 159-163.
12. King, M.K., "Comment on 'Spin Effects on Rocket Nozzle Performance,"' ***Journal of Spacecraft and Rockets.*** Vol. ***3.*** No. 12. December 1966, pp. 1812-1813.
13. King, W.S., "On Swirling Nozzle Flows," *Journal* of ***Spoacecraft and Rockets,*** Vol. 4, No. 10, October 1967, pp. 1404-1405.
14. Manda, L.J., "Spin Effects on Rocket Nozzle Performance," ***Journal*** of ***Spacecraft and Rockets,*** Vol. 3, No. 11, November 1966, pp. 1695-1696.